

Article

Optimum Synthesis of a BOA Optimized Novel Dual-Stage $PI - (1 + ID)$ Controller for Frequency Response of a Microgrid

Abdul Latif ^{1,*}, S. M. Suhail Hussain ² , Dulal Chandra Das ¹  and Taha Selim Ustun ² 

¹ Department of Electrical Engineering, National Institute of Technology Silchar, Assam 788010, India; dulal@ee.nits.ac.in

² Fukushima Renewable Energy Institute, AIST (FREIA), National Institute of Advanced Industrial Science and Technology (AIST), Koriyama 963-0298, Japan; suhail.hussain@aist.go.jp (S.M.S.H); selim.ustun@aist.go.jp (T.S.U.)

* Correspondence: abdul_rs@ee.nits.ac.in

Received: 3 June 2020; Accepted: 1 July 2020; Published: 3 July 2020



Abstract: A renewable and distributed generation (DG)-enabled modern electrified power network with/without energy storage (ES) helps the progress of microgrid development. Frequency regulation is a significant scheme to improve the dynamic response quality of the microgrid under unknown disturbances. This paper established a maiden load frequency regulation of a wind-driven generator (WG), solar tower (ST), bio-diesel power generator (BDPG) and thermostatically controllable load (heat pump and refrigerator)-based, isolated, single-area microgrid system. Hence, intelligent control strategies are important for this issue. A newly developed butterfly algorithmic technique (BOA) is leveraged to tune the controllers' parameters. However, to attain a proper balance between net power generation and load power, a dual stage proportional-integral- one plus integral-derivative $PI - (1 + ID)$ controller is developed. Comparative system responses (in MATLAB/SIMULINK software) for different scenarios under several controllers, such as a proportional-integral (PI), proportional-integral-derivative (PID) and $PI - (1 + ID)$ controller tuned by particle swarm optimization (PSO), grasshopper algorithmic technique (GOA) and BOA, show the superiority of BOA in terms of minimizing the peak deviations and better frequency regulation of the system. Real recorded wind data are considered to authenticate the control approach.

Keywords: isolated hybrid microgrid system ($IH\mu GS$); solar tower (ST); biodiesel power generator (BDPG); frequency regulation; butterfly optimization technique (BOA); microgrid energy management

1. Introduction

Electricity consumption is increasing in parallel with population and energy demand [1]. The increasing generation capacity with conventional energy sources has negative impacts on environment [2]. Research shows that the introduction of microgrids with renewable energy resources (RERs) is an environmentally friendly solution to this energy problem [3,4].

Microgrids can provide energy in a clean and optimal way when digital control technologies are coupled with sources such as wind and solar. However, the intermittent characteristics of RERs and low inertia of inverter-interfaced systems cause control and stability issues in microgrids [5]. Hence, combining diesel generators and RERs [6–8] is one possible solution to mitigate the detrimental effects (e.g., frequency fluctuation) of hybrid power systems. Additionally, a non-toxic bio-diesel power generator (BDPG) can be a more environment-conscious supplementary option for frequency regulation schemes.

To overcome the frequency fluctuation in a more reliable way, different storage devices (SDs) have been considered, such as battery (BSD), fuel cell (FCSD), ultra-capacitor (UCSD) and superconducting magnetic storage system (SMSD) [9]. There are maintenance and disposal concerns for BSD, while FCSD suffers from slow response and SMSU experiences leakage of expensive helium liquid [10]. In the following, a cost-effective, carbon-neutral-based, solid-oxide fuel cell (SOFC) can be utilized for the frequency regulation of isolated hybrid microgrids (*IH μ GS*). In addition, different thermostatically controllable loads (TCLs) such as a heat pump (*HP*) and refrigerator (*RFZ*) are employed for smoothing the dynamic system responses. In the recent past, several studies have focused on the frequency regulation of *IH μ GS* [11–15]. The study in [12] framed out a mathematical modeling of a system comprised of dish-stirling, solar thermal, diesel and SDs. The authors of [13] sketched a load frequency management for a hybrid power system that includes wind, solar PV and SDs. In fact, the application of a plug-in electric vehicle (PHEV)-battery (BSD) to contain frequency fluctuation is investigated in [14].

Beside the system architectures, several works have introduced a load frequency controller such as proportional-integral (*PI*) [9], proportional-integral-derivative (*PID*) [6], model predictive controller (MPC) [16], fractional order *PID* (FOPID) [17] or PIFOD [18] for the aforementioned issues. In this work, a dual-stage, proportional-integral-one plus integral-derivative $PI - (1 + ID)$ controller is introduced for the provision of better system dynamics.

Several algorithmic techniques have been leveraged in order to optimally tune the controller parameters for *IH μ GSs*, such as genetic algorithm (GA) [9], PSO [6], firefly technique (FA) [19], cuckoo search technique (CS) [14], mine blast technique (MBA) [20], grasshopper algorithmic technique (GOA) [21]. A comprehensive review of different algorithmic techniques for a load frequency controller is presented in [22]. In this regard, this work explores the application of a butterfly algorithmic tool (BOA) for designing the parameters of a frequency controller. This algorithm was recently developed and is considered in this paper due to its high convergence rate [23].

Therefore, the scope of this work and its contributions to the current body of knowledge can be summarized as follows:

- (a) Developing a frequency controller for a *WG-ST-BDPG-SOFC-HP-RFZ*-based *IH μ GS*;
- (b) To establish a new transfer function model of a dual-stage $PI - (1 + ID)$ controller;
- (c) Comparative system dynamic analysis of different controllers such as *PI*, *PID* and $PI - (1 + ID)$ controllers under a BOA algorithmic tool;
- (d) Comparative system dynamic analysis of different algorithms (PSO, GOA and BOA), leveraging the acquired superior controller in (c);
- (e) Study system dynamics under real recorded wind data and other random disturbances.

The rest of the paper is organized as follows: Section 2 details the frequency response modeling steps. Section 3 gives an overview of the BOA technique and shows its adaptation for the purposes of this work. It also presents the proposed dual-stage controller. Simulation works and their analyses are presented in Section 4. The conclusions are given in Section 5.

2. Frequency Response Modeling of the Proposed Dual-Stage Controller

The hybrid system of the proposed work consists of wind generators (1.5 MW); solar-tower-based, solar-thermal power system (1 MW), *BDPG* (800 kW), *SOFC* (200 kW); thermostatically controllable *HP*; *RFZ* elements; and demanded loads (2.2 MW). The schematic layout and abbreviation of the relevant parameters are shown in Figure 1 and Table 1, respectively.

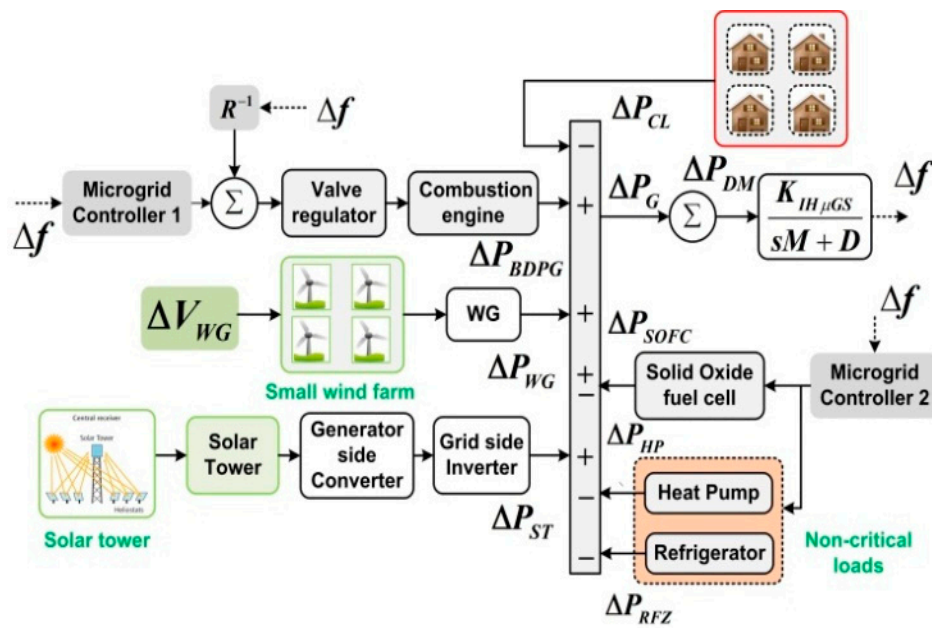


Figure 1. Schematic representation of $IH\mu GS$.

Table 1. Utilized symbols and abbreviations.

Symbol	Nomenclature	Value
ΔP_{CL}	Change in critical load power in p.u.	-
Δf	Aberration of frequency in Hz	-
ΔP_G	Change in net generated power	-
ΔP_{DM}	Change in net power difference from ΔP_G and ΔP_{CL}	-
K_{VR}	Gain of Valve actuator	1
K_{BE}	Engine gain	1
T_{VR}	Valve regulator delay time	0.08 s
T_{CE}	Time constant of bio-diesel power generator (BDPG)	0.4 s
K_{WG}	Gain of wind-driven generator (WG)	1
T_{WG}	Time constant of WG	5 s
K_{RF}, K_{RV}	Gain value of refocus and receiver	1, 1
K_G, K_T	Gain value of governor and turbine	1, 1
T_{RF}, T_{RV}	Time constant of refocus and receiver	1.33 s, 4 s
T_G, T_T	Time constant of governor and turbine	0.08 s, 1 s
K_{SOFC}	Gain of solid-oxide fuel cell (SOFC)	1
T_{SOFC}	Time constant of SOFC	0.2 s
K_{HP}	Gain of heat pump (HP)	1
T_{HP}	Time constant of HP	0.1 s
K_{RFZ}	Gain of refrigerator (RFZ)	1
T_{RFZ}	Time constant of RFZ	0.265 s
t_{sim}	Simulation time of $IH\mu GS$	100 s

2.1. Wind Generator (WG)

The kinetic energy of the wind converts into electrical energy through the wind generator (WG). As wind is a highly variable source, the power output through the WG depends on the instantaneous speed of the wind. Equation (1) formulates how wind energy is converted to the mechanical output power of WG.

$$P_{WG} = 0.5 \cdot V_{WG}^3 \cdot \rho \cdot A_{bd} \cdot C_P(\lambda, \beta) \quad (1)$$

where ρ , V_{WG} , A_{bd} , and C_P are, in proper order, the air density, intermittent wind speed, blade-swept area and the extractable power co-efficient. Akkanayakanpatti station's recorded wind speed data are

considered and modelled in the proposed work [24]. The rate of change in real recorded wind power (ΔP_{WG}) and transfer function model of the WG are represented as shown in Equation (2) [25]

$$\Delta P_{WG} = \begin{cases} 0, & V_{WG} < V_{cut-in} \text{ or } V_{WG} > V_{cut-out} \\ 0, & V_{rated} \leq V_{WG} \leq V_{cut-out} \\ ([0.007872 V_{WG}^5 - 0.23015 V_{WG}^4 + 1.3256 V_{WG}^3 \\ + 11.061 V_{WG}^2 - 102.2 V_{WG} + 2.33] \cdot \Delta V_{WG}), & \text{else} \end{cases} \quad (2)$$

$$G_{WG}(s) = \frac{K_{WG}}{sT_{WG} + 1}$$

2.2. Solar Tower (ST)

The dual-axis (vertical and horizontal) heliostats-enabled central receiver system is *ST*, placed on a surface. Here, the reflected solar radiation is focused on the central receiver of *ST* with a higher concentration ratio (500–1000) and temperature (500–850 °C) of fluid (steam or molten salt). The collected incident solar power (P_{in}) can be deliberated as

$$P_{in} = \eta_h \cdot I \cdot A_h \quad (3)$$

where A_h is the heliostats area, I incident solar radiation and η_h is the system constant. By solving the state equations, the linearized transfer function model of *ST* can be represented as [18]

$$G_{ST}(s) = \left(\frac{K_{RF}}{sT_{RF} + 1} \right) \cdot \left(\frac{K_{RV}}{sT_{RV} + 1} \right) \cdot \left(\frac{K_G}{sT_G + 1} \right) \cdot \left(\frac{K_T}{sT_T + 1} \right) \quad (4)$$

2.3. Biodiesel Power Generator (BDPG)

The combination valve regulator and combustion-engine-based biodiesel power generation (*BDPG*) was leveraged to offer support as a backup power generation. It has inherently biodegradable and non-toxic positive characteristics, which were the main reasons to incorporate it in the suggested work. Equation (5) details the transfer function of *BDPG* [21].

$$G_{BDPG}(s) = \left(\frac{K_{VR}}{sT_{VR} + 1} \right) \cdot \left(\frac{K_{CE}}{sT_{CE} + 1} \right) \quad (5)$$

2.4. Solid-Oxide-Based Fuel Cell (SOFC)

Through the electrochemical reaction, the fuel cell produces dc power and, by using a DC-AC converter, this power is converted into AC. With a fast charging–discharging time and higher efficiency (~80%), the *SOFC* has gained much interest in recent years among all the categories of FCSDs. In view of the above, *SOFC* was selected as the storage device in the system. Its transfer function model is given in Equation (6) [18]

$$G_{SOFC}(s) = \frac{K_{SOFC}}{sT_{SOFC} + 1} \quad (6)$$

2.5. Thermostatically Controllable Loads (HP and RFZ)

In order to manage the energy consumption and to improve the system dynamic responses (by controlling operation cycles), two thermostatically controllable loads were considered, i.e., heat pump (*HP*) and *RFZ*. The transfer function models of *HP* [19] and *RFZ* [19] could be expressed as in Equations (7) and (8)

$$G_{HP}(s) = \frac{K_{HP}}{sT_{HP} + 1} \quad (7)$$

$$G_{RFZ}(s) = \frac{K_{RFZ}}{sT_{RFZ} + 1} \quad (8)$$

2.6. IHμGS Dynamic Model

The instantaneous change in power (ΔP_G) of the proposed IHμGS can be formulated as

$$\Delta P_G = \Delta P_{WG} + \Delta P_{ST} + \Delta P_{BDPG} \pm \Delta P_{SOFC} - \Delta P_{NCL} = \Delta P_{CL} \rightarrow 0 \quad (9)$$

where

$$\begin{aligned} \Delta P_{NCL} &= \Delta P_{HP} + \Delta P_{RFZ} \\ \text{and } \Delta P_{DM} &= \Delta P_G - \Delta P_{CL} \end{aligned} \quad (10)$$

The equivalent dynamic model of IHμGS could be illustrated as

$$G_{IH\mu GS}(s) = \left(\frac{\Delta f}{\Delta P_{DM}} \right) = \frac{K_{IH\mu GS}}{D + sM} \quad (11)$$

Refer to Table 1 for the nomenclature and abbreviations used for IHμGS system modelling.

2.7. Objective Function Formulation

The formulation of the objective function (J) has a great impact on system dynamics and the achieved results. Therefore, the proposed work considered the integral of square error (ISE) objective function. This could be formulated as

$$\text{Minimize } J_{ISE} = \int_0^{t_{sim}} (\Delta f)^2 .dt \quad (12)$$

Subject to :

$$\left\{ \begin{array}{l} K_{Pi}^{\min} \leq K_{Pi} \leq K_{Pi}^{\max} \\ K_{li}^{\min} \leq K_{li} \leq K_{li}^{\max} \\ K_{Di}^{\min} \leq K_{Di} \leq K_{Di}^{\max} \\ K_{li2}^{\min} \leq K_{li2} \leq K_{li2}^{\max} \\ K_{Di2}^{\min} \leq K_{Di2} \leq K_{Di2}^{\max} \end{array} \right. \quad (13)$$

where $i = 1, 2$. The range of controller parameters is taken as (0–50).

3. Optimization Techniques

Three metaheuristic techniques were considered to optimally tune the controller parameters along with their comparative dynamic responses.

3.1. Particle Swarm Technique (PSO)

A swarm-based metaheuristic particle swarm technique (PSO) was developed by Eberhart and Kennedy in 1995 to solve the specified problem by improving the candidate solution with reference to the given measure quality [26]. The solution of PSO is termed as a particle. Every particle follows a track of coordinates in the problem space until the best solution is reached with respect to the suggested problem. The velocity of each particle is varied on the basis of best position (P_{best}) and I_{best} location. The optimum values obtained by optimizer are termed as I_{best} [26].

3.2. Grasshopper Algorithmic Technique (GOA)

A metaheuristic grasshopper algorithmic technique was proposed by Saremi et al. [27]. Its characteristics depend on the swarming and foraging characteristics of grasshopper, which could be modeled to form structural algorithmic techniques. The steps involved for initialization, exploitation and exploration are depicted in [27].

3.3. Butterfly Optimization Technique (BOA) and Proposed Dual-Stage Controller

Recently, since 2018, based on the food-probing approach and mating characteristics of butterflies, a nature-inspired algorithmic technique named BOA has been developed to solve several engineering problems. The unique food-probing strategy and mating characteristics of BOA are modeled in [23].

The main idea of BOA depends on three key parameters. These are sensor modality (M_s), impulsive intensity (I_s) and power component (γ). Moreover, the objective function of this technique depends on the distinction of I_s and formation of fragrance (P), which could be formulated as

$$P_i = M_s \cdot I_s^\gamma \quad i \in (1, 2, \dots, N) \quad (14)$$

where P_i is the fragrance magnitude of i th butterfly. In the following, to investigate global search stage, a dominated fitted solution q^* could be depicted as

$$m_i^{t+1} = m_i^t + (n^2 \times q^* - m_i^t) \cdot P_i \quad (15)$$

where $n \in [0, 1]$

where m and q^* are the solution vectors of i th butterfly and current best solution among all the solutions. The formulation of the social search could be illustrated as

$$m_i^{t+1} = m_i^t + (n^2 \cdot m_g^t - m_h^t) \cdot P_i \quad (16)$$

where, m_g and m_h are the g th and h th butterflies enabled in the search space [23]. The approximate flow diagram of BOA technique is framed out in Figure 2. All the parameters considered for algorithmic techniques are given in Appendix A.

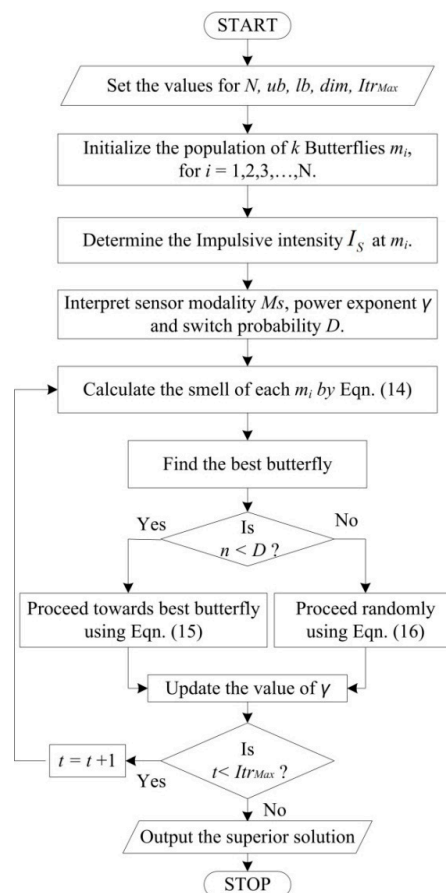


Figure 2. Flow diagram of butterfly optimization technique (BOA).

To reach above control target, a novel dual-stage proportional-integral-integral-derivative ($PI - (1 + ID)$) controller is deployed, as framed in Figure 3. In the following, Δf is leveraged as an input signal, whereas $C(s)$ is the output control signal of the controller. The control output signal and transfer function of the proposed controller are formulated as

$$C(s) = \Delta f \cdot PI - (1 + ID) \quad (17)$$

$$G_{PI-(1+ID)}(s) = K_P + K_I/s - (1 + K_I/s + K_D \cdot s) \quad (18)$$

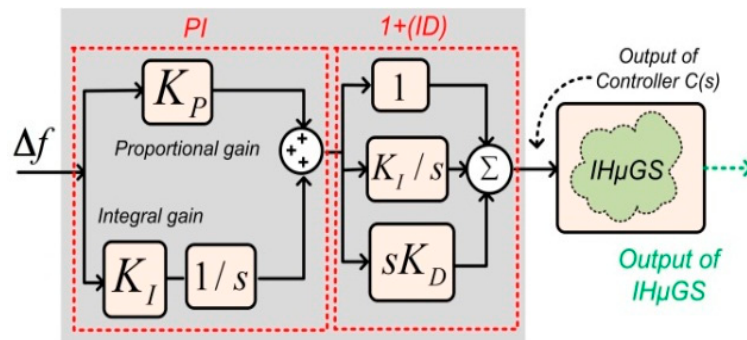


Figure 3. Proposed ($PI - (1 + ID)$) controller.

4. Frequency Response Studies and Analysis

In order to verify the proposed control strategy, two scenarios are simulated in a system with Core-i7-4770 CPU under MATLAB/SIMULINK (R2013a, MathWorks, Natick, USA) was environment. Three algorithmic techniques (PSO, GOA and BOA) have been considered. Furthermore, to validate the control strategy, real recorded wind speed data have been considered.

4.1. Scenario 1: Performance Analysis of All Controllers during Non-Accessibility of All RERs

In this scenario, assume that all the RERs are unavailable due to maintenance. Therefore, the extractable power forms WG (ΔP_{WG}) and ST (ΔP_{ST}) are zero ($\Delta P_{WG} = \Delta P_{ST} = 0\%$) during the entire period. A net constant critical load demand ($\Delta P_{CL} = 30\%$) is considered from $t = 0$ s onwards. The comparative performance of different controllers such as PI , PID and ($PI - (1 + ID)$) are displayed in Figure 4, where the tuned parameters are listed in Table 2. The system dynamics assessment of the abovementioned controllers under BOA and objective function (J_{ISE}) and figure of demerits (J_{FOD}) clearly depicts that the proposed ($PI - (1 + ID)$) controller is superior to the rest. To elaborate further, the performance indicators such as peak overshoot ($+O_P$), peak undershoot ($-U_P$) and settling time (T_{ST}) are tabulated in Table 2.

Table 2. Comparative performance parameters of different controllers with optimal BOA-tuned gain values.

Controllers	PI	PID	$PI - (1 + ID)$
Peak Overshoot(+O_P)			
ΔF (in Hz)	0.0544	0.0136	0.0006
Peak Undershoot(-U_P)			
ΔF (in Hz)	0.0669	0.0389	0.0190
Settling Time (T_{ST})			
ΔF (in s)	3.976	4.097	2.581

Table 2. Cont.

Controllers		PI	PID	PI – (1 + ID)
Minimization of $J (J_{min})$				
		7.79×10^{-4}	2.92×10^{-5}	2.91×10^{-5}
Figure of Demerits (J_{FOD})				
		15.816	16.787	6.662
Optimal Controller Parameters				
Controller-1	K_{P1}	3.010	0.502	0.325
	K_{I1}	5.103	12.11	10.702
	K_{D1}	-	0.108	-
	K_{I12}	-	-	0.513
	K_{D12}	-	-	0.118
Controller-2	K_{P2}	18.116	5.001	1.508
	K_{I2}	20.207	5.509	4.109
	K_{D2}	-	1.624	-
	K_{I22}	-	-	1.128
	K_{D22}	-	-	2.219

Bolt point out superior output.

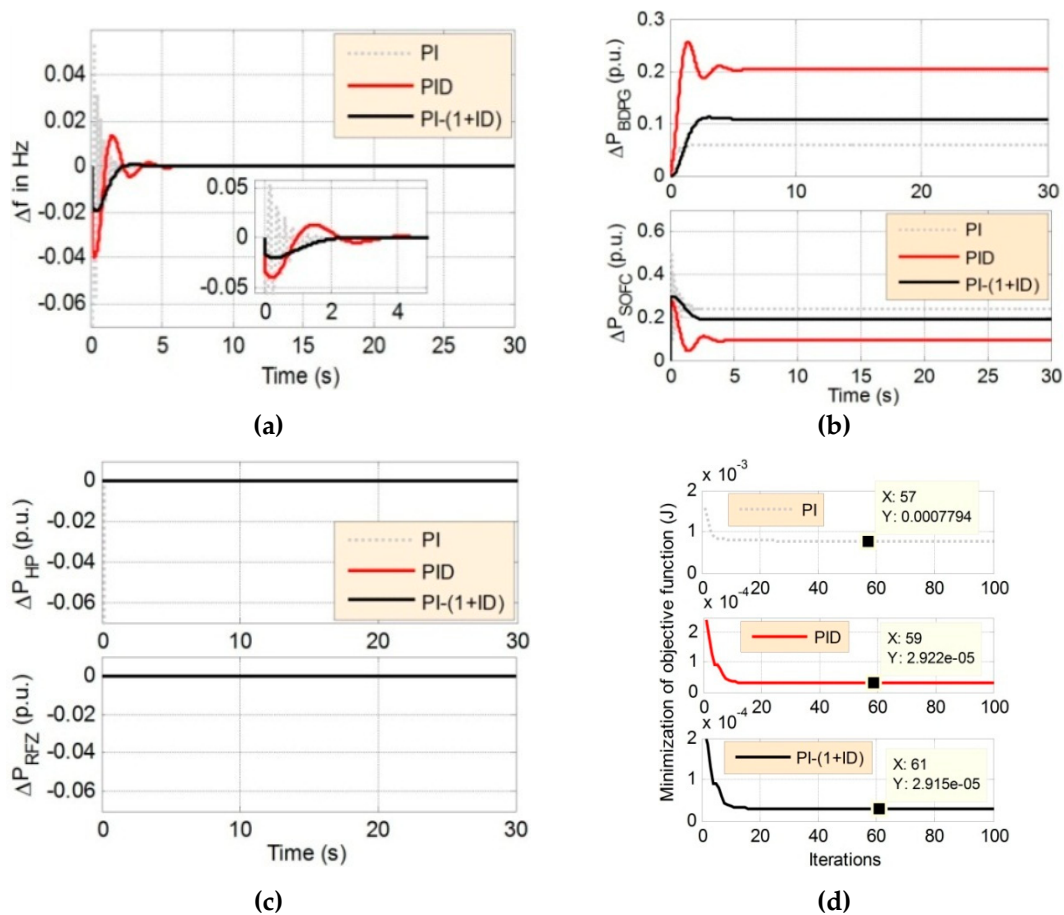


Figure 4. Comparative system dynamics analysis of different controllers (proportional-integral (PI), PI-derivative (PID), (PI – (1 + ID))) (a) deviation in system frequency (Δf), (b) change in extractable power of bio-diesel power generator (BDPG) and SOFC, (c) change in extractable power of HP and RFZ, (d) Comparative converged objective function (J_{min}).

4.2. Scenario 2: Performance analysis of Different Algorithms Under Concurrent Random Changes of WG (Utilization of Real-Recorded Data), ST and Critical Load Demand

In this scenario, the proposed system is tested under real-recorded wind (obtained from National Institute of Wind Energy, India) [25], as displayed in Appendix B. The operating condition is illustrated with 30% average power of ST and 50% critical load demand for the entire time duration. The wind speed and its corresponding output power is shown in Figure 5a. The results are depicted in Figure 5b–e, showing the comparative system dynamic responses of Δf , ΔP_{BDPG} , ΔP_{SOFC} , ΔP_{HP} , and ΔP_{RFZ} . Figure 5b–e it clearly shows that the BOA-optimized $PI - (1 + ID)$ controller performed better than the other suggested PSOs, GOA-tuned ($PI - (1 + ID)$) controller. The tuned values of the controller parameters are displayed in Table 3.

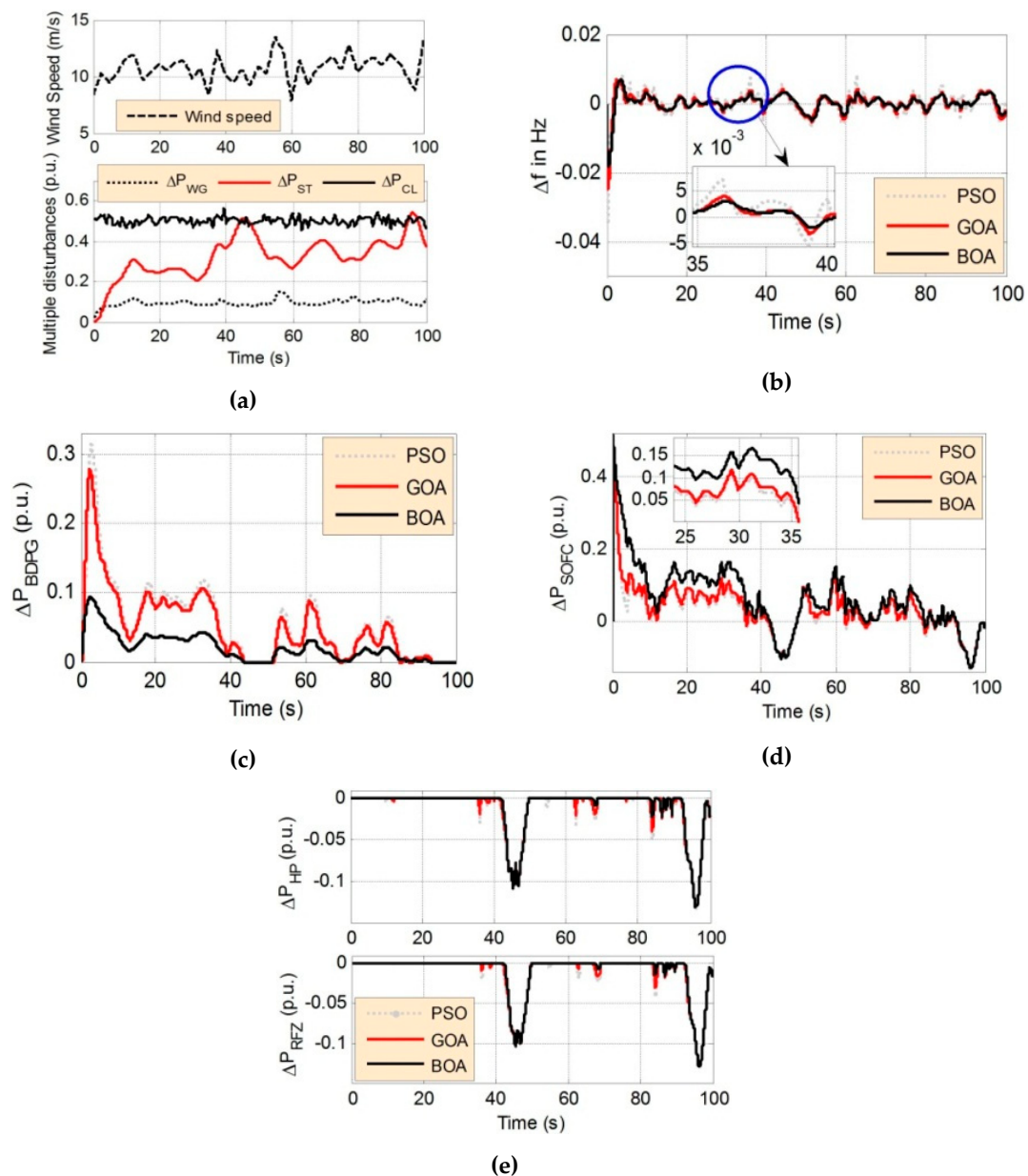


Figure 5. Comparative system dynamics analysis of different algorithmic techniques (PSO, GOA, BOA) (a) Real recorded wind speed and other multiple disturbances, (b) deviation of system frequency (Δf), (c) change in extractable power of BDPG, (d) change in extractable power of SOFC, (e) change in extractable power of HP and RFZ.

Table 3. Optimal values of particle swarm optimization (PSO), grasshopper algorithmic technique (GOA) and BOA techniques tuned $PI-(1+ID)$ controller.

Techniques		PSO	GOA	BOA
Optimal controller parameters				
Controller-1	K_{P1}	0.3112	0.2986	0.3210
	K_{I1}	5.0070	20.051	25.053
	K_{I12}	0.5021	0.5170	0.5087
	K_{D12}	0.1085	0.1153	0.1078
Controller-2	K_{P2}	0.5170	2.5171	4.6087
	K_{I2}	4.1850	4.1751	4.1098
	K_{I22}	1.1190	1.2015	1.1069
	K_{D22}	2.2191	2.2276	2.2183

5. Conclusions

The present article develops a novel frequency regulation scheme for wind-solar-tower-biodiesel-based $IH\mu GS$. A novel dual-stage ($PI - (1 + ID)$) controller is enabled to investigate the system dynamics under different scenarios. A recently developed BOA technique is utilized to optimally tune the proposed dual stage ($PI - (1 + ID)$) controller gains and compare the system dynamics under real recorded wind data. The comparative system dynamic responses, as well as performance parameters such as peak deviation ($+O_p$, $-U_p$) and settling time (T_{ST}), clearly indicate that the BOA-optimized ($PI - (1 + ID)$) controller performs better than other classical benchmark controllers. The simulation test results prove the effectiveness of the proposed control strategy. This control scheme could be further extended by integrating different RER technologies and storage devices, as well as electric vehicles, into the microgrid.

Author Contributions: Conceptualization, A.L., S.M.S.H., D.C.D. and T.S.U.; Methodology, A.L., S.M.S.H., D.C.D. and T.S.U.; Software, A.L.; Validation, A.L.; Formal Analysis, A.L., S.M.S.H., D.C.D. and T.S.U.; Writing—Original Draft Preparation, A.L. and D.C.D.; Writing—Review and Editing, S.M.S.H., and T.S.U.; Visualization, A.L.; Supervision, D.C.D.; Funding Acquisition, T.S.U. All authors have read and agreed to the published version of the manuscript.

Funding: This research received no external funding.

Acknowledgments: Authors would like to thank TEQIP-III NIT Silchar for providing technical support for this work.

Conflicts of Interest: The authors declare no conflict of interest.

Appendix A

PSO technique: Number of population: 50, Maximum iteration (Itr_{Max}): 100, Max^m weight factor (W_{max}): 0.9, Min^m weight factor (W_{min}): 0.1, Acceleration factors (C1&C2): 2.

GOA technique: Number of population: 50, Maximum iteration (Itr_{Max}): 100, Maximum coefficient factor (C_{fmax}) = 1, Minimum coefficient factor (C_{fmin}) = 0.00004, attraction intensity (f): 0.5, length scale of attractiveness (l): 1.5

BOA technique: Number of population: 50, Maximum iteration (Itr_{Max}): 100, Probability of switching (D) = 0.8, Power component (γ) = 0.1, Sensor modality (Ms) = 0.1.

Appendix B

WG: Date of noted data: 1st July, 2016, Minimum speed of wind: 7.4804 m/s; Maximum speed of wind: 14.08 m/s; Average speed of wind: 10.922 m/s; SD: 1.1895.

References

1. Global Energy Review 2020, International Energy Agency (IEA), Paris. 2020. Available online: <https://www.iea.org/reports/global-energy-review-2020> (accessed on 2 July 2020).
2. Global Energy & CO2 Status Report 2019, International Energy Agency (IEA), Paris. 2019. Available online: <https://www.iea.org/reports/global-energy-co2-status-report-2019> (accessed on 2 July 2020).
3. Xie, H.; Zheng, S.; Ni, M. Microgrid Development in China: A method for renewable energy and energy storage capacity configuration in a megawatt-level isolated microgrid. *IEEE Electr. Mag.* **2017**, *5*, 28–35. [[CrossRef](#)]
4. Ustun, T.S.; Nakamura, Y.; Hashimoto, J.; Otani, K. Performance analysis of PV panels based on different technologies after two years of outdoor exposure in Fukushima, Japan. *Renew. Energy* **2019**, *136*, 159–178. [[CrossRef](#)]
5. Dong, X.; Zhang, X.; Jiang, T. Adaptive Consensus Algorithm for Distributed Heat-Electricity Energy Management of an Islanded Microgrid. *Energies* **2018**, *11*, 2236. [[CrossRef](#)]
6. Das, D.C.; Sinha, N.; Roy, A.K. Automatic Generation Control of an Organic Rankine Cycle Solar-Thermal/Wind-Diesel Hybrid Energy System. *Energy Technol.* **2014**, *2*, 721–731. [[CrossRef](#)]
7. Dhillon, S.S.; Lather, J.S.; Marwaha, S. Multi objective load frequency control using hybrid bacterial foraging and particle swarm optimized PI controller. *Int. J. Electr. Power Energy Syst.* **2016**, *79*, 196–209. [[CrossRef](#)]
8. Ghafouri, A.; Milimonfared, J.; Gharehpetian, G.B. Fuzzy-adaptive frequency control of power system including microgrids, wind farms, and conventional power plants. *IEEE Syst. J.* **2017**, *12*, 2772–2781. [[CrossRef](#)]
9. Das, D.C.; Roy, A.K.; Sinha, N. GA based frequency controller for solar thermal-diesel-wind hybrid energy generation/energy storage system. *Int. J. Electr. Power Energy Syst.* **2012**, *43*, 262–279. [[CrossRef](#)]
10. Nadeem, F.; Hussain SM, S.; Tiwari, P.K.; Goswami, A.K.; Ustun, T.S. Comparative Review of Energy Storage Systems, Their Roles, and Impacts on Future Power Systems. *IEEE Access* **2019**, *7*, 4555–4585. [[CrossRef](#)]
11. Singh, K.; Amir, M.; Ahmad, F.; Khan, M.A. An Integral Tilt Derivative Control Strategy for Frequency Control in Multimicrogrid System. *IEEE Syst. J.* **2020**. [[CrossRef](#)]
12. Das, D.C.; Sinha, N.; Roy, A.K. Small signal stability analysis of dish-Stirling solar thermal based autonomous hybrid energy system. *Int. J. Electr. Power Energy Syst.* **2014**, *63*, 485–498. [[CrossRef](#)]
13. Hussain, I.; Ranjan, S.; Das, D.C.; Sinha, N. Performance Analysis of Flower Pollination Algorithm Optimized PID Controller for Wind-PV-SMES-BESS-Diesel Autonomous Hybrid Power System. *Int. J. Renew. Energy Res.* **2017**, *7*, 643–651.
14. Latif, A.; Pramanik, A.; Das, D.C.; Hussain, I.; Ranjan, S. Plug in hybrid vehicle-wind-diesel autonomous hybrid power system: Frequency control using FA and CSA optimized controller. *Int. J. Syst. Assur. Eng. Manag.* **2018**, *9*, 1147–1158. [[CrossRef](#)]
15. Khooban, M.H.; Gheisarnejad, M. A Novel Deep Reinforcement Learning Controller Based Type-II Fuzzy System: Frequency Regulation in Microgrids. *IEEE Trans. Emerg. Top. Comput. Intel.* **2020**. [[CrossRef](#)]
16. Pahasa, S.; Ngamroo, I. Coordinated Control of Wind Turbine Blade Pitch Angle and PHEVs Using MPCs for Load Frequency Control of Microgrid. *IEEE Syst. J.* **2016**, *10*, 97–105. [[CrossRef](#)]
17. Latif, A.; Das, D.C.; Ranjan, S.; Barik, A. Comparative performance evaluation of WCA-optimised non-integer controller employed with WPG-DSPG-PHEV based isolated two-area interconnected microgrid system. *IET Renew. Power Gener.* **2019**, *13*, 725–736. [[CrossRef](#)]
18. Latif, A.; Das, D.C.; Barik, A.K.; Ranjan, S. Maiden co-ordinated load frequency control strategy for ST-AWEC-GEC-BDDG based independent three-area interconnected microgrid system with the combined effect of diverse energy storage and DC link using BOA optimized PFOID controller. *IET Renew. Power Gener.* **2019**, *13*, 2634–2646. [[CrossRef](#)]
19. Ray, P.K.; Mohanty, A. A robust firefly-swarm hybrid optimization for frequency control in wind/PV/FC based microgrid. *Appl. Soft Comput.* **2019**, *85*, 105823. [[CrossRef](#)]
20. Atawi, I.E.; Kassem, A.M.; Zaid, S.A. Modeling, Management, and Control of an Autonomous Wind/Fuel Cell Micro-Grid System. *Processes* **2019**, *7*, 85. [[CrossRef](#)]
21. Barik, A.; Das, D.C. Expeditious frequency control of solar photobiotic/biogas/biodiesel generator based isolated renewable microgrid using grasshopper optimisation algorithm. *IET Renew. Power Gener.* **2018**, *12*, 1659–1667. [[CrossRef](#)]

22. Latif, A.; Hussain, S.M.S.; Das, D.C.; Ustun, T.S. State-of-the-art of controllers and soft computing techniques for regulated load frequency management of single/multi-area traditional and renewable energy based power systems. *Appl. Energy* **2020**, *266*, 114858. [[CrossRef](#)]
23. Arora, S.; Singh, S. Butterfly optimization algorithm: A novel approach for global optimization. *Soft Comput.* **2019**, *23*, 715–734. [[CrossRef](#)]
24. Wind Speed Data. Available online: http://niwe.res.in:8080/NIWE_WRA_DATA/DataTable_D4.jsf (accessed on 2 July 2020).
25. El-Fergany, A.A.; El-Hameed, A.M. Efficient frequency controllers for autonomous two-area hybrid microgrid system using social-spider optimizer. *IET Gener. Transm. Distrib.* **2017**, *11*, 637–648. [[CrossRef](#)]
26. Dutta, D.; Figueira, J.R. Graph partitioning by multi-objective real-valued metaheuristic: A comparative study. *Appl. Soft Comput.* **2011**, *11*, 3976–3987. [[CrossRef](#)]
27. Saremi, S.; Mirjalili, S.; Lewis, A. Grasshopper optimization algorithm: Theory and application. *Adv. Eng. Softw.* **2017**, *105*, 30–47. [[CrossRef](#)]



© 2020 by the authors. Licensee MDPI, Basel, Switzerland. This article is an open access article distributed under the terms and conditions of the Creative Commons Attribution (CC BY) license (<http://creativecommons.org/licenses/by/4.0/>).